

*Invited Paper***Mode splitting in the terahertz functional devices: a review**

Lin Chen, Yiming Zhu* and Songlin Zhuang

Shanghai Key Lab of Modern Optical System, Engineering Research Center of Optical Instrument and System,
Ministry of Education, University of Shanghai for Science and Technology,
516, Jungong Rd. Yangpu Dist. Shanghai, China, 200093

* Email: ymzhu@usst.edu.cn

(Received January 20, 2014)

Abstract: The mode splitting effect was observed widely in different waveguide structures in Terahertz (THz) field and has great potentiality to achieve the high quality THz functional devices. This review discusses various THz functional waveguide devices based on mode splitting and analyzes the physical origins of such phenomena.

Keywords: Terahertz functional device, Mode splitting, Frequency selective surface

doi: [10.11906/TST.080-099.2014.06.07](https://doi.org/10.11906/TST.080-099.2014.06.07)

1. Introduction

In recent years, with the development and blossom of the application of THz technology, huge potential applications in different many fields have been found and realized [1-10], such as biotechnology, space science, terahertz wave communications, medical imaging and plasma diagnostics. It is vital and necessary to manufacture THz components, such as filter, slow light device, and frequency selective surface and other functional devices [1, 2]. Those functional devices are based on various structures, such as grating [3], photonic crystals [4] surface plasmon polaritons [5] and quantum well [6]. In this paper, several useful and easily fabricating THz functional devices based on mode splitting are introduced, which have potential applications for high Q THz filters, high bio-detection resolution, etc.

Firstly, a metal hole arrays (MHA) structure fabricated on aluminum slab can be used as High Q THz filter of wide frequency range. This type of MHA is based on extraordinary optical transmission caused by surface plasmon polaritons (SPPs). Further research indicates the oblique incidents around the vertical and horizontal axes making the transmission peaks split into two resonant peaks according to the break of symmetry in broad sense, which is a different mechanism from metamaterial. Then, a multi-cavity resonant system made by silicon wafers and stainless spacer is a potential device to realize the THz wavelength division multiplexing (WDM) due to three equidistant channels observed in the experiment. These three channels are formed by superposing symmetrical and asymmetrical hybridizing of eigenmodes of sub-structures i.e. the single cavities. By adjusting the incident angle, the device can tune the central frequencies of the three transmission channels. Afterwards, an asymmetric waveguide-cavity system based on metal

parallel plate waveguide (PPWG) has electromagnetically induced transparency (EIT) phenomenon in the THz range. The widths of two transmission dips can easily be changed by varying the shift length between two identical grooves fabricated on the two metal blocks. Experiment results show the transmissivity of two dips are both less than 5%. It's a very efficient band-stop filter. Eventually, a frequency selective surface (FSS) composed of connected electric LC resonators for polarization modulation purpose has been investigated. Then a single unit of this device comprises 4 square ELC structures and 2 connecting bent-lines and the device is fabricated on a flexible PI substrate with a copper layer. The device shows very different status at 45° and 135° depending on whether the bent-lines exist. This feature is useful for the fabrication of narrow band polarization modulator.

Furthermore, most of these devices are measured by using high performance time domain terahertz spectroscopy system [11-15], which is also made in University of Shanghai for Science and Technology, as shown in Fig. 1. In this system, we use m-i-n diode as the terahertz emitter [11-14], whose frequency can reach 4.2 THz and the scan speed can reach 10 scan/s .

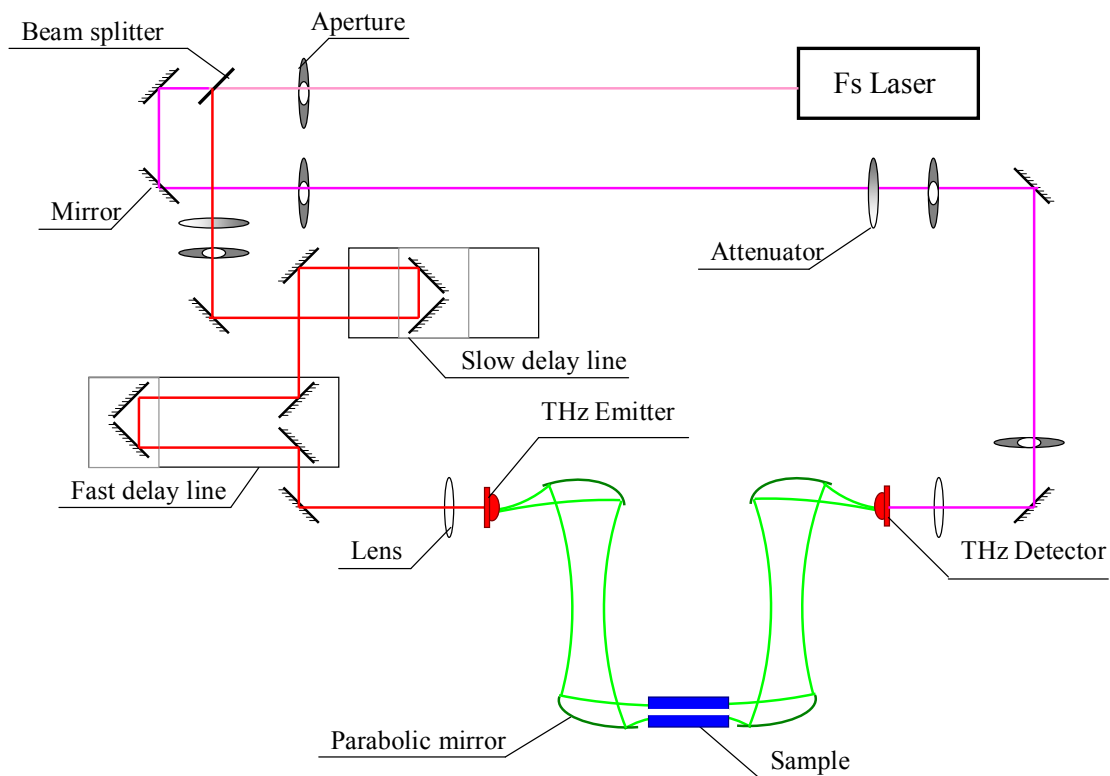


Fig. 1 Optical layout of THz-TDS in transmission configuration.

2. Metal holes array [15, 16]

Metal holes array (MHA) is the holes array fabricated on metal slab. In this study, to better

understand the characteristics of surface waves and mode splitting, the relationship between the incident angle and the transmission of surface waves through a metal holes array (MHA) structure was investigated. In contrast with the mode splitting of near-field coupling coming from electromagnetically induced transparency in asymmetrical metamaterial systems, the mode splitting effect observed in this study depends on the in-plane component of the incidence vector. In addition, two splitting modes also have different properties: the high-order mode excited by a coupled mode of surface waves and the hole modes have a shorter attenuation length than that of the low-order mode, which is excited just by the spoof surface plasmons. A theoretical model is established to explain these characteristics. Our results harness the full potential of MHAs, which can find many applications in THz devices.

To excite surface waves, we fabricate an aluminum MHA slab as shown in Fig. 2. Traditional micromachining is used to fabricate the arrays. Using a stepping motor control system, the spacing of the holes can be measured precisely. The MHA slab consists of a triangular array of circular air holes on a $t = 250 \text{ mm}$ thick, $50 \text{ mm} \times 50 \text{ mm}$ rectangular aluminum plate. The holes have a diameter of $d = 0.7 \text{ mm}$ and are arranged on a hexagonal lattice with a pitch of $s = 1.13 \text{ mm}$. The number of holes is large enough in our structure to avoid the finite size effect.

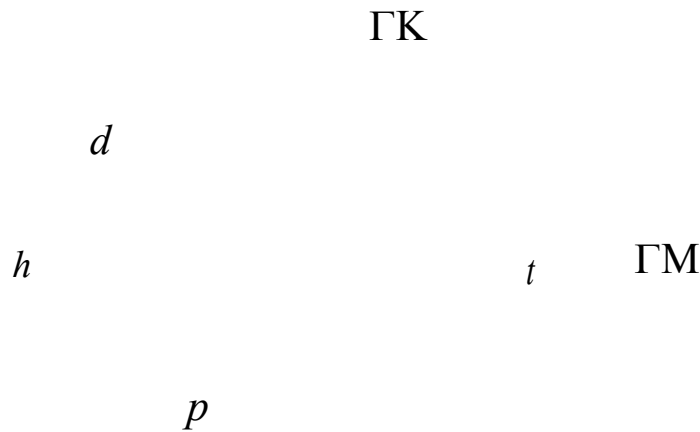


Fig. 2 Schematic diagram of a MHA

A transmitted pulse is measured using a THz time domain spectroscopy. A collimated p-polarized THz wave, which is radiated from a 100 fs & 800 nm laser pulse pumped photoconductive antenna emitter, is irradiated on the MHA. We rotate the MHA around its axis, as shown in Fig. 2, to vary the in-plane vector of the incident wave in the ΓM direction. By varying the time delay between the pumping and probe pulses, the waveform of the transmitted THz wave can be measured. An empty air signal is used as a reference for our measurements.

Firstly, we investigate the effect of periodical extension on transmission characteristics of MHA [15].

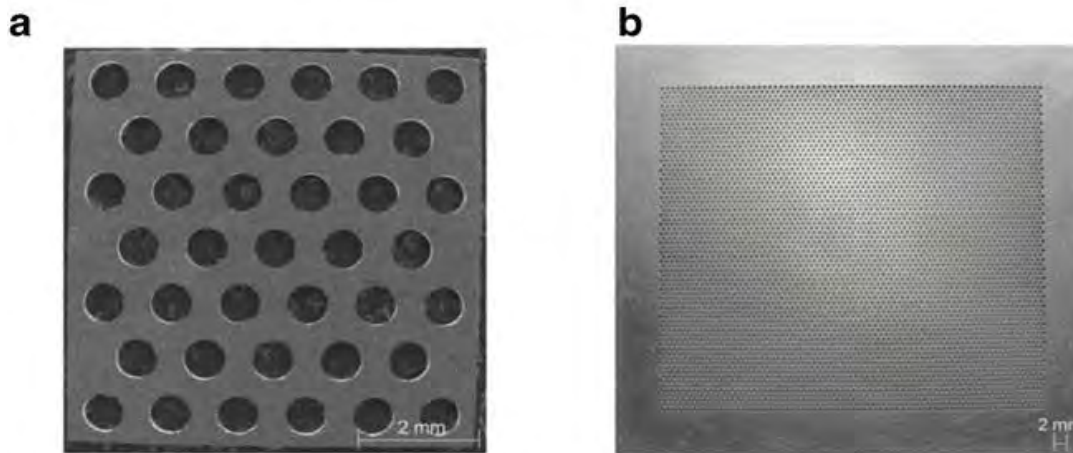


Fig. 3 SEM image of MHA sample of different sizes and scales, (a) small-size sample with 39 holes on $6 \times 6 \text{ mm}$, (b) big-size sample with more than 5000 holes on $100 \times 100 \text{ mm}$

Fig. 3 shows the SEM image of the hole arrays. Fig. 3 (a) is the photo image of the small-size sample with 39 holes on $6 \text{ mm} \times 6 \text{ mm}$ aluminum slab. Fig. 3 (b) is the photo image of the big-size sample with more than 5,000 holes on $100 \text{ mm} \times 100 \text{ mm}$ aluminum slab and margin in the edge of slab, whose size is almost 278 times bigger than the small sample.

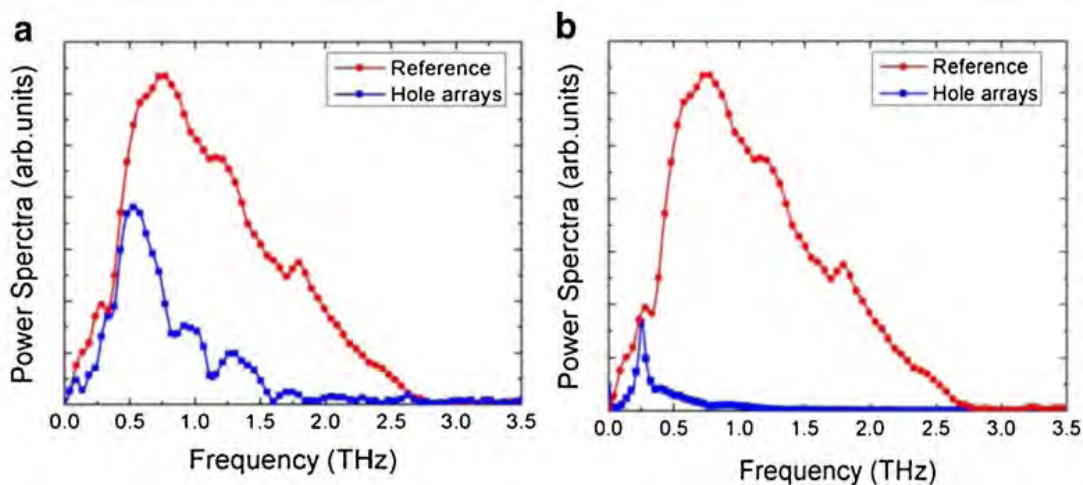


Fig. 4 The reference (red) and sample (blue) spectra of small and big size MHA sample

Fig. 4 (a) shows the reference THz signal (red curve) and the THz waveform transmit through the big-size sample (blue curve) in time domain. Similar with the small-size sample case, the amplitude of THz signal through the big-size sample decreases. It is also obvious that five damped oscillations occur after the main peak, whose period is about 3.75 ps . The spectra of reference signal and the transmitted signal from the big-size sample are shown in Fig. 4 (b). The filtering effect is also clearly observed. By comparing with the amplitude of $E_{\text{THz}}(\omega)$ for both the reference signal and the signal from the big-size sample at 0.26 THz , we can find that the

transmission efficiency of big-size sample (more hole arrays) is about 95 %. The difference between the calculated and experimental results of small-size sample mainly comes from the insufficient periodical extension and boundary condition.

So, we use a big-sized sample to verify the mode splitting effect [16]. For comparison, we have studied the MHA at normal incidence ($\theta=0^\circ$). After inserting the MHA, the signal shows an additional off-plane oscillating attenuation tail, which is probably originated from the interaction between the incident waves and the surface waves on the metal surface. To characterize this oscillation, we perform a Fourier transformation to obtain spectra of the frequency domain. The resonant peak of the normal incidence is located at 0.265 THz. According to Pendry's theory, the cutoff frequency represents the marginal value of the spoof surface plasma frequency. The experimental results show that the resonant frequency is larger than the cutoff frequency. Therefore, spoof surface plasmon polariton theory cannot be applied directly to our MHA at normal incidence.

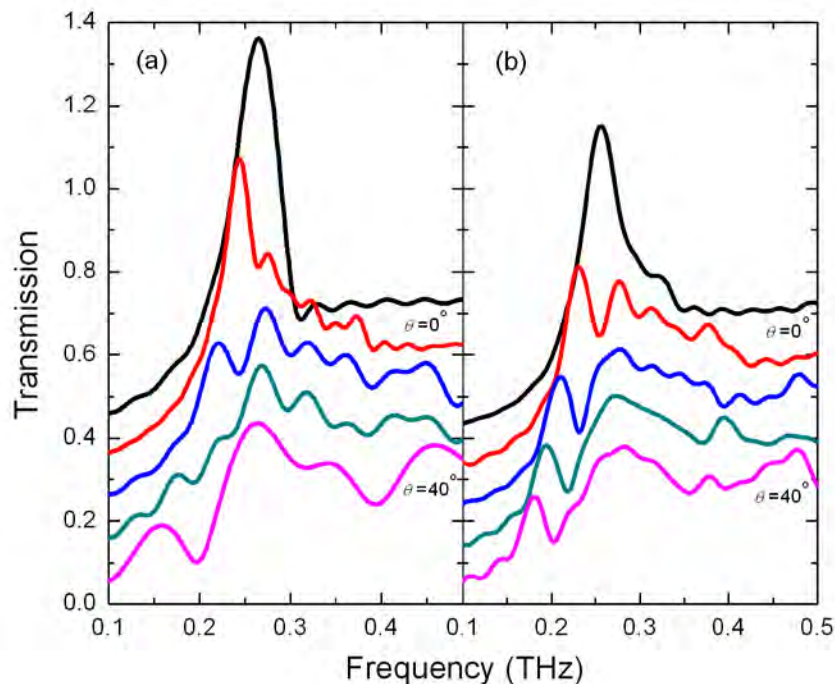


Fig. 5 Transmission spectra of the MHA at incident angles, (a) Experimental; (b) numerical results

We then conduct an experimental study on the angular-dependent transmission features of the MHA, and the results of which are shown in Fig. 5 (a). We find that by changing the incident angle θ , the resonant peak of the surface wave splits into two peaks, one with a lower frequency and the other with a higher frequency relative to the frequency of the non-split peak at an incident angle of 0° . Moreover, the low-frequency peak moves toward lower frequencies as the incident angle increases. We also perform numerical calculations on the transmission spectra using CST software, inputting the same parameters used in the experiment; the results are shown in Fig.5 (b). The calculation results show similar behavior to those observed in the experiments. We also

measure the transmission spectra by rotating the MHA around the ΓM axis to obtain a variation of the in-plane component in the ΓK direction and obtained similar results. We attribute this phenomenon to the excitation of surface waves. The surface wave vector will couple with the in-plane vector of the incident wave on the MHA slab at a finite incident angle.

To quantitatively analyze the transmission spectra that are dependent on the incident wave vector direction, a surface wave dispersion relationship is used. This dispersion relationship is appropriate for smooth metal/dielectric surfaces, therefore, the influence of the hole arrays is neglected for convenience in performing the calculations. If an incident wave is irradiated on a grating at an angle of θ , the energy and momentum conservation of the coupling effect between the surface wave and the incident wave vector is given by:

$$\mathbf{k}_{sw} = \mathbf{k}_{in} + m\mathbf{G}_x + n\mathbf{G}_y \quad (1)$$

where \mathbf{k}_{sw} is the surface wave vector; \mathbf{k}_{in} is the in-plane vector of the incident wave; m and n are integers; \mathbf{G}_x and \mathbf{G}_y represent the grating momentum.

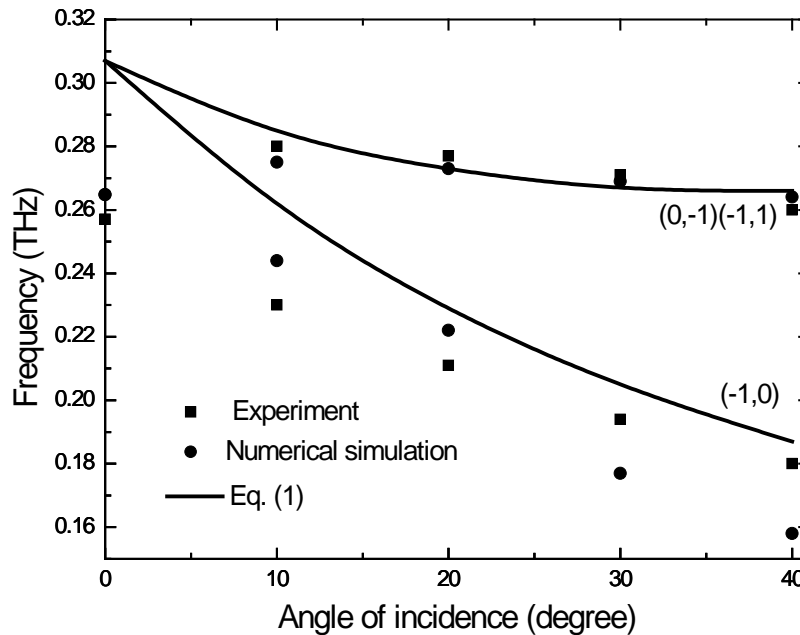


Fig. 6 Dispersion relationship of modes (-1,0) and (0,-1) (-1,1).

As Shown in Fig.6, when the incident angle θ becomes finite, the lowest mode splits into two branches. These newly emerged branches are excited as a result of the non-zero parallel vector of the incident wave. For an accurate estimate of the shift in surface wave resonances, we analyze the position of the strongest transmission peak modes, (-1,0) and (0,-1)/(-1,1). Here, the (0,-1) and (-1,1) modes are degenerate, and both have the same dispersion relationship according to (1). The dispersion curves for the surface wave modes (-1,0) and (0,-1)/(-1,1) are displayed in Fig. 6. The numerical and experimental results extracted from Fig. 5 are also presented. The

experimental results agree well with the numerical results and the results of the calculations performed using (1). From (1), we can also see that k_{in} increases or decreases with the reciprocal vectors, which depend on the incident angle. The in-plane wave vector k_{in} increases with the incident angle θ , leading to a shift in the photonic bands to lower frequencies. The physical origins of this phenomenon lie in the folding of the in-plane Brillouin zone and have been discussed in detail by Ghaemi et al. with respect to the visible range. The splitting characteristics clearly confirm the involvement of surface wave excitation during the transmission process. For high-order peaks beyond 0.4 THz, this splitting characteristic is very weak. This is because the reciprocal vectors of high-order modes are sufficiently large and less sensitive to the variation of the in-plane vector of the incident wave.

3. Silicon-based resonance system [17]

A high-quality triple-channel terahertz filter based on silicon multi-cavity resonant system has been experimentally investigated by using backward wave oscillator. Theoretical methods have been employed to analyze physical origin of the resonances and the transmission properties. We find that the lower transmission peak comes from the Fabry-Perot resonance in the side, and the two thick cavities and the higher two peaks are caused by the symmetrically and asymmetrically coupling of the two thin cavities in the middle. The resonant peaks show blue shift by increasing the incident angle, which is attributed to the change of effective refractive indices.

Recently, the filter based on one-dimension (1-D) photonic crystals (PCs) with one defect has been widely studied due to their HQ feature, simple configuration and low cost. The central frequency of the filter can also be tuned by adjusting the thickness of the defect layers. The phenomenon can be explained by the Fabry-Perot resonant (FPR) effect of multilayer structure. However, due to the large number of periods, the maximum transmissivities of the filters based on PCs are unsatisfactory. On the contrary, THz multi-cavity resonant system with the small number of periods has the advantages of multiple channels and high transmissivities, which makes this type of structure to be the potential devices to realize the THz wavelength division multiplexing (THz-WDM). However, the interaction of more than two cavities (especially two cavities with different thickness) and its physical origin in formation of transmission have few been reported. In this study, we design, simulate and analyze a multi-cavity resonant system which has three HQ transmission peaks. We use results from both calculation and simulation to analyze the mechanism in the formation of all three peaks observed in the experiment. We indicate the interactions exist between any two cavities among these four different cavities: two cavities of same thickness, two cavities of different thickness, and even two cavities which do not adjoin. Besides, the influences of different incident angles on three resonant frequencies are also discussed, which caused by the change of effective refractive indices.

The aim of our study is to find a low-cost and easily fabricated filter with good transmission

properties. Considering the fact that the more difference of two material's refractive indices (n) is, the stronger the FPR effect is, we choose silicon ($n = 3.42$) and air ($n = 1$) to fabricate our sample.

The transfer matrix method (TMM) has been used to design sample as calculation method. According to TMM, the entire sample can be described by a transfer matrix of all layers as [18]:

$$\begin{pmatrix} E_{in} \\ H_{in} \end{pmatrix} = M \begin{pmatrix} E_{out} \\ H_{out} \end{pmatrix}, \quad (2)$$

where the transfer matrix of entire sample M is the product of the transfer matrix of each layer M_i :

$$M = \begin{pmatrix} m_{11} & m_{12} \\ m_{21} & m_{22} \end{pmatrix} = \prod_i M_i, \quad i = 1, 2, 3, \dots \quad (3)$$

and in the i th layer,

$$M_i = \begin{pmatrix} \cos(k_i l_i) & j \eta_i \sin(k_i l_i) \\ \frac{j}{\eta_i} \sin(k_i l_i) & \cos(k_i l_i) \end{pmatrix}, \quad (4)$$

In the equations, j is the imaginary unit ($j^2 = -1$), and the subscription i implies the physical quantity concerned in the i th layer. n_i , l_i , $k_i = n_i k_0$ and η_i stand for the refractive index, the thickness, the wave vector and the relative wave impedance in the i th layer, respectively. The refractive index n_i can be written as $n_i = \sqrt{\epsilon_i}$ and $\epsilon_i = 1$ for air, $\epsilon_i = 11.87 - 0.006j$ (lossy) for silicon.

The reflectance r and transmittance t for field strength can be calculated by the elements of the transfer matrix¹³.

$$r = \frac{m_{11} + m_{12} - m_{21} - m_{22}}{m_{11} + m_{12} + m_{21} + m_{22}} \quad t = \frac{n_{in}}{n_{out}} \frac{2}{m_{11} + m_{12} + m_{21} + m_{22}} \quad (5)$$

where, n_{in} and n_{out} are the refractive indices of materials on the input and output sides of sample. The sample in experiment is in the air with $n_{in} = n_{out} = 1$. The reflectivity R and transmissivity T for light intensity are the square of modulus of the two coefficients i.e., $R = rr^*$ and $T = tt^*$ (“*” means conjugation).

The sample that we have fabricated consists of five $\sim 3 \times 3 \text{ cm}^2$ square pieces of silicon cut from single Si wafer with high resistance and four stainless spacers of different thicknesses (shown in Fig. 7). The sheet resistance, crystal orientation, thickness and diameter of wafer are 20000~28000 Ω , $\langle 100 \rangle \pm 0.5^\circ$, $525 \pm 15 \mu\text{m}$ and $100 \pm 0.3 \text{ mm}$, respectively. The four stainless

spacers are used: two are 1.04 mm -thick and others are 0.94 mm -thick. A metal clip is used to sandwich the pieces and spacer of the multi-cavity resonant structure. As shown in Fig. 7, in the experiment, we also use two 0.5 mm -thick spacer to distribute the pressure of the clip. Considering the flatness, stiffness and effective contact area of wafers and spacer, the thickness difference between top and bottom has controlled to ensure the precise of sample.

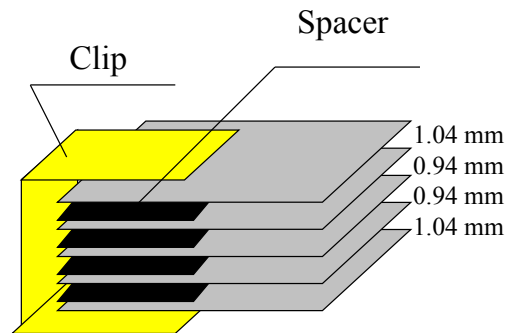


Fig. 7 The structure of the sample

In the experiment, a backward wave oscillator (BWO) made by MicroTech Instruments is used as the THz emitter to investigate the transmission properties of sample. The center frequencies of the radiation can be adjusted from 231 GHz to 380 GHz and the average output power approximately equals to 15 mW . Our sample is 10 cm away from emitter and 15 cm away from the detector in the experiment. A Teflon lens is set close behind the sample to focus the THz wave and an alternate attenuator is set to protect the detector. The frequency ranging from 270 GHz to 330 GHz is chosen in experiment considering the potential positions of transmission peaks, where three peaks appear in calculation. The humidity and temperature are controlled at $\sim 10\%$ and $\sim 24^\circ\text{C}$ in whole experiment.

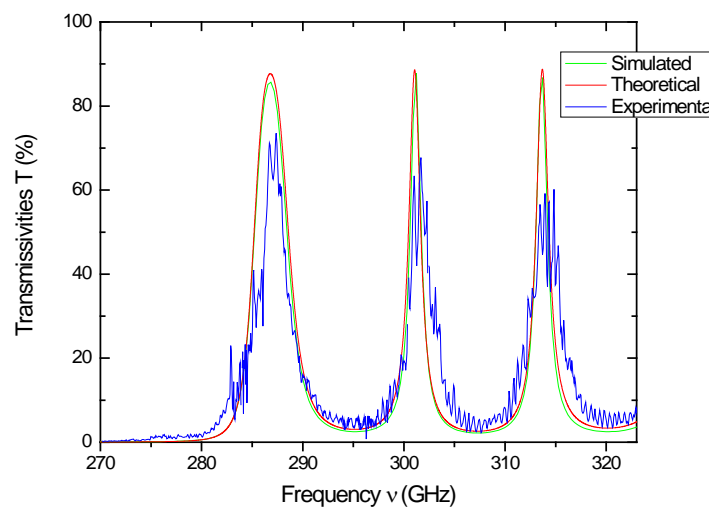


Fig.8 Transmission curves at normal incidence obtained via different ways, *green line*: simulated, *red line*: theoretical, *blue line*: experimental

After post-processing, the transmission curve for normal incidence measured in experiment is illustrated in Fig. 8 with the blue line. For comparison, the calculated result by TMM and simulated one by COMSOL Multiphysics® with “*RF Module/In-Plane Waves*” are both illustrated in Fig. 8 with the red and green lines, respectively. The four main transmission properties of three transmission peaks observed in experiment and calculation are also listed in Tab. I. The experimental results show that the sample we have designed is a THz filter with high transmissivities ($\sim 70\%$), triple quasi-equidistant channels ($\sim 14\text{ GHz}$), narrow peaks ($\sim 3\text{ GHz}$) and high quality ($\sim 100x$). Experimental results agree with theoretical and simulated ones.

Tab. I The transmission properties of three transmission peaks

Orders of Transmission peaks	Experimental			Theoretical		
	1st	2nd	3rd	1st	2nd	3rd
Central frequency ν_0 (GHz)	286.94	301.68	314.84	286.80	301.06	313.68
Maximum T (%)	73.54	67.75	60.17	87.70	88.62	88.76
FWHM $\Delta\nu$ (GHz)	3.303	1.779	2.669	3.732	1.392	1.506
Quality factor Q (x)	86.87	169.60	117.98	76.84	216.26	208.27

This phenomenon can be explained by the theory of resonant mode coupling. In the theory, the whole sample can be treated as a Fabry-Perot resonator. As shown in Fig. 9, the configuration of this structure can be divided into four single-cavity resonant systems. Two of them consist of two silicon wafers and a 1.04 mm-thick cavity (SAS), and others consist of two silicon wafers and a 0.94 mm-thick cavity (SRS). The central frequencies of transmission peaks for each single-cavity system can be decided by considering the FPR effect. By calculation with TMM, the central frequencies of two type single-cavity system (SAS & SRS) are 289.38 GHz and 304.08 GHz. The two eigenmodes of single-cavity resonant system are denoted as $|\omega_1\rangle$ and $|\omega_2\rangle$ in Dirac notation system. However, in our experiment, because of their close positions, the two thin cavities in the middle can act as a coupling tunnel between the two thick cavities. There are two kinds of the coupling methods for the middle cavities: symmetrically and asymmetrically, which should make the eigenmode $|\omega_2\rangle$ split into two new modes (denoted as $|\omega_-\rangle$ and $|\omega_+\rangle$). Besides, the two thick cavities on the side can simply superpose by each other (new mode denoted as $|\omega_0\rangle$). Considering the energy of asymmetric coupling modes is lower than symmetric ones intrinsically and the energy of $|\omega_1\rangle$ is lower than $|\omega_2\rangle$ because of its larger cavity thickness, the peaks whose central frequencies are 286.80 GHz, 301.06 GHz, and 313.68 GHz in theoretical calculation are corresponding to $|\omega_0\rangle$, $|\omega_-\rangle$ and $|\omega_+\rangle$, respectively (the relative energy levels of all modes mentioned are shown as the vertical position in Fig. 9). We find the central frequencies of $|\omega_-\rangle$ (301.06 GHz) and $|\omega_+\rangle$ (313.68 GHz) are not symmetrical to the cone of eigenmode $|\omega_2\rangle$. Further research shows that the asymmetrical location of split modes central frequencies observed in experiment is depended on more complex mechanism.

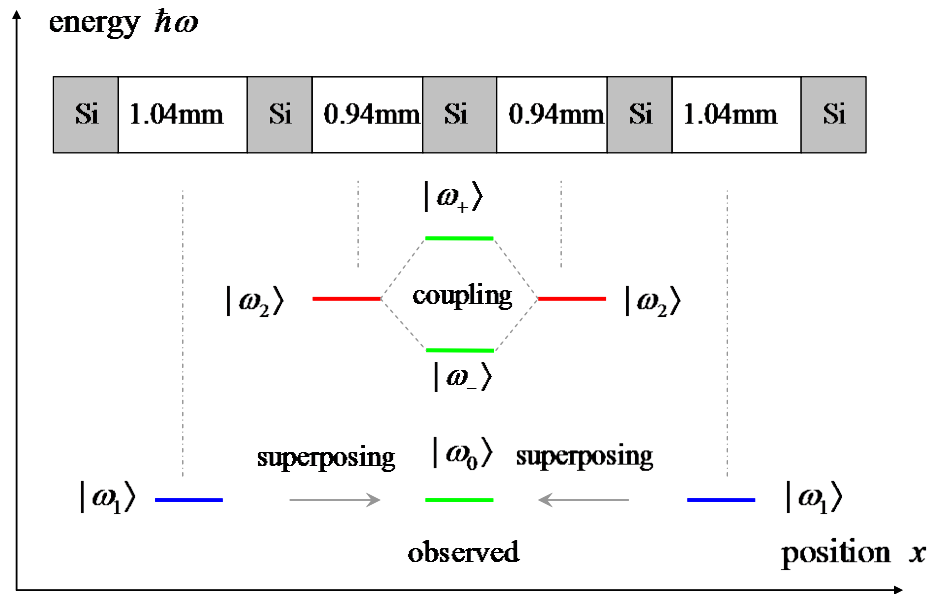


Fig. 9 The analysis chart of modes formation

The mechanism of the shift of the central frequencies in main structure SASRSRSAS is clear. The eigenmode $|\omega_2\rangle$ (for SRS) splits into two modes, $|\omega_-\rangle$ and $|\omega_+\rangle$ (for SRSRS) by symmetrically and asymmetrical coupling. Adding two additional thick cavities on the side (SASRSRSAS) will generate three split modes: the lower resonant mode $|\omega_0\rangle'$ comes from the eigenmode $|\omega_1\rangle$ (for SAS); the higher two resonant modes $|\omega_-\rangle'$ and $|\omega_+\rangle'$ come from $|\omega_-\rangle$ and $|\omega_+\rangle$ (for SRSRS). The interaction between the thin and thick resonance cavities makes the central frequencies shift ($|\omega_0\rangle$ to $|\omega_0\rangle'$, $|\omega_-\rangle$ to $|\omega_-\rangle'$ and $|\omega_+\rangle$ to $|\omega_+\rangle'$, as shown in Fig. 9), which indeed generates three transmission observed in all of experiment, calculation and simulation (blue line in Fig. 9).

4. Parallel plate waveguide [19, 20]

The parallel plate waveguide (PPWG) is a potential electromagnetically induced transparency (EIT) device in THz range. The realization of this EIT in atomic systems is a tough task since some restrictions must be strictly fulfilled. So mimicking EIT in classical systems has been continuously done. In the field of optics, waveguide based EIT-like resonances have been proposed numerically in resonant cavity systems. Importantly, the phase coupling between the resonators has been proved to be a key factor for EIT-like response [21, 22]. In THz region, a plasmon-induced transparency (PIT) that relies on the strength of near-field coupling of metallic cavities has been observed in asymmetric metamaterial systems. However, tuning the physical parameters of THz meta-materials after fabrication is a huge challenge. A metal PPWG in the THz regime is intensively studied due to its superior confining effect for the propagating THz waves. The PPWG with a single cavity has also been found to be a strong and high Q resonant system in which a transverse electric (TE_1) mode can be excited. These unique properties of the

PPWG-cavity system probably offer a way for achieving waveguide-based EIT. In this Letter, we report an observation of an EIT-like phenomenon in THz PPWG cavities systems and analyze the relation between the off-position of the cavities and the transmission properties. The proposed system has the following features: first, since the most popular metals are seen as perfect conductors due to extremely large conductivity in the THz region, the realization of THz EIT-like response in PPWG-cavities systems is not plasmonically induced. Second, the two cavities have identical geometry; therefore, the detuning of resonant frequencies does not arise from the different geometrical parameters of two cavities. We find the EIT-like transmission presented here results from the resonance hybridization induced by the change of coupling strength of top and bottom cavities [19]. We also find that two detuned resonances (the symmetric and asymmetric resonances) can be varied by choosing different shifting length between two cavities. This means that phase shift of the propagating wave between two resonances may be another important factor for the realization of EIT. The physical picture of an analogy to the coupling of bright and dark modes in THz meta-materials is also presented.

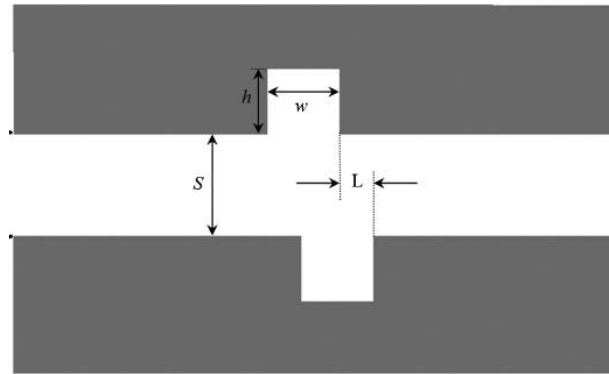


Fig. 10 Schematic of PPWG with two cavities

The PPWG-cavities system consists of two aluminum plates, each with a micro-machined rectangular groove (cavity), as shown in Fig. 10. All cavities have the identical geometry with a width $w = 470 \mu\text{m}$ ($\pm 5 \mu\text{m}$) and a depth $h = 420 \mu\text{m}$ ($\pm 5 \mu\text{m}$). We fabricate four sets of PPWG cavities configurations: a perfect symmetric one with the top and the bottom cavities exactly at the center of the waveguide and asymmetric configurations made by keeping the top cavity fixed and displacing the bottom cavity from the center position with $L = 0, 100, 200, 300 \mu\text{m}$, respectively, where L represents the bottom cavity shifting length from the center in the propagation direction. S represents the length of the plates. Combined fast and slow scan-based THz time domain spectroscopy (THz-TDS) is used for evaluating the transmission properties of the PPWG system. The fast optical delay line with 110 ps range can be obtained. If we combine it with slow scan, the overall delay line can be expanded to 218.4 ps. This means the experimental spectra resolution can be achieved to 4.58 GHz. The electric field of the incident beam is oriented parallel to the plates in order to excite the TE_1 mode.

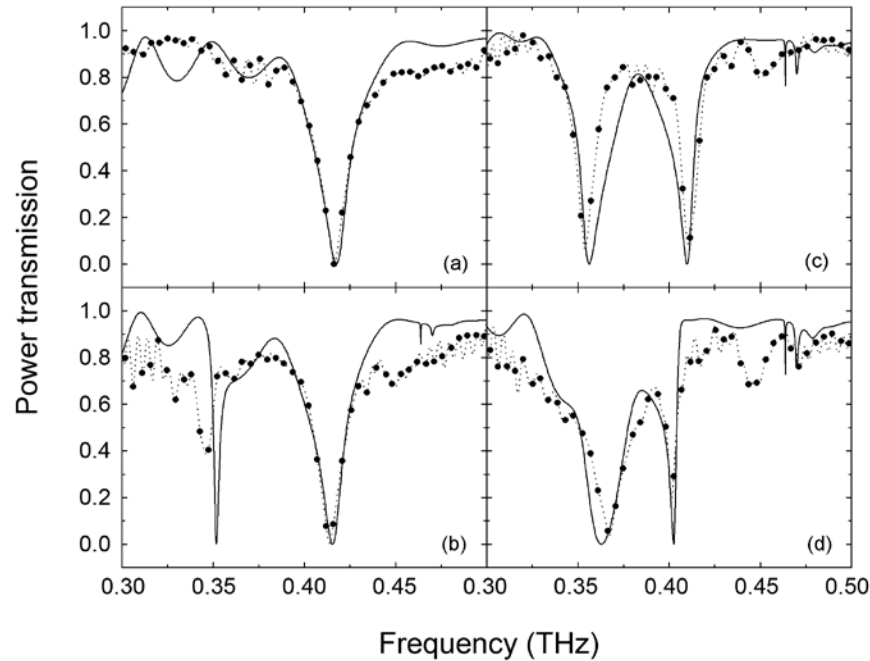


Fig. 11 the Fourier-transformed intensity of the THz wave forms, *solid line*: simulated, *dash line & dots*: experimental, (a)-(d) stand for $L = 0, 100, 200, 300 \mu\text{m}$

Next, we discuss the influence of the shifting length L on the transmission response. For this discussion, the length of the top and bottom plates is fixed at $S = 650 \mu\text{m}$. The PPWG without any cavity acts as the reference. Fig. 11 shows the power transmission of the PPWG-cavities system with different L . For the structure with symmetry ($L = 0 \mu\text{m}$), only one broad symmetric resonant dip at 0.417 THz was observed. For the PPWG cavities structure with $L = 100 \mu\text{m}$, asymmetry is introduced, resulting in a new resonant dip at lower frequency (0.354 THz). When the bottom cavity is further shifted up to $L = 200 \mu\text{m}$, the lower resonant frequency shows blue shift and the high resonant frequency shows red shift. A transparent band between two resonant dips becomes narrow as well as the decrease of the transmittance. Here, we observe an EIT-like transmission that is similar to previous investigations for metamaterial and plasmon analogues of EIT. For the asymmetric structure with $L = 300 \mu\text{m}$, two resonance dips come closer and the transmission peak reduces further. The experimental results agree well with numerical results in Fig. 11 and the deviation is probably caused by the fabrication imperfections of the sample, which introduce further asymmetry and rearrangement of some resonant frequencies. For a complete picture of resonant frequencies change, several calculations are performed with the variation of the shifting length from 0 to $450 \mu\text{m}$. The detuning $|\omega_1 - \omega_2|$ (ω_1 and ω_2 are low and high resonant frequencies, respectively) decreases and the transparency window narrows down with the increase of the shifting length L .

This EIT-like transmission can also be explained by analogy to the coupling of bright and dark modes. When the bottom cavity is set symmetrically to the top one, only one resonant dip, which corresponds to the two bright modes (each of them has the same resonant frequency), can be

excited in both cavities simultaneously. In this condition, the dark mode cannot be excited. When the bottom cavity is shifted backward from the symmetric position, due to the identical geometry of the two cavities, the incident wave first arrives at the top cavity and couples with it. The shifted bottom cavity can hardly be interacted directly with the incident wave anymore but can couple with the top cavity. In other words, the top cavity acts as the “radiative” resonator (a bright mode) that is coupled to a “bus” waveguide; the bottom cavity acts as the “sub-radiant” resonator (a quasi-dark mode, induced by the shifting length of two cavities) that cannot be coupled to the “bus” waveguide. This physical picture is similar to the unit cell (consists of an upper gold strip as a bright mode, a pair of lower gold strips as a dark mode, and a dielectric spacer) described in. Then this EIT-like transmission can also be seen as the coupling between bright and quasi-dark modes when the symmetry is broken.

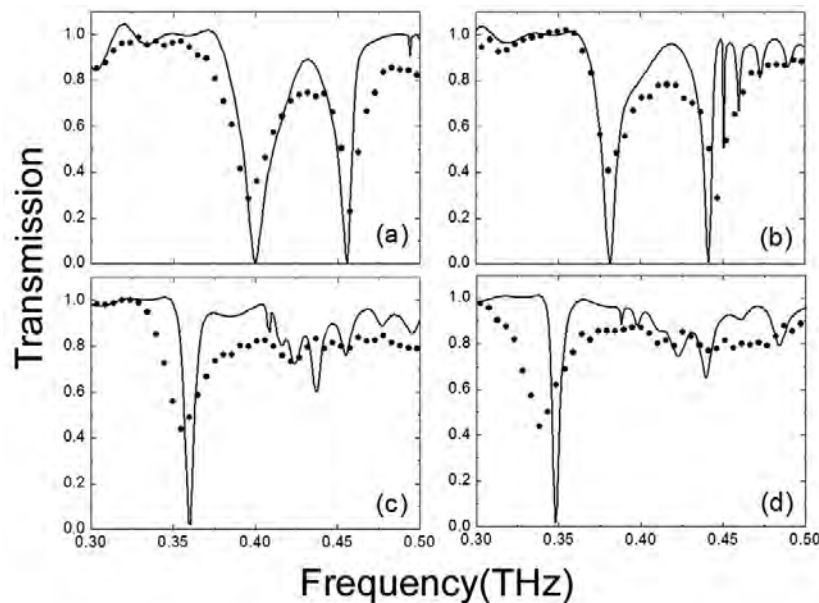


Fig. 12 Measured THz spectra with various air gaps, *solid line*: simulated, *dots*: experimental, (a)-(b) stand for $S = 610, 670, 740,$ and $780 \mu\text{m}$

Besides, the influence of the length of the top and bottom plates S is also investigated [20]. Four different waveguide spacings, with $S = 610, 670, 740,$ and $780 \mu\text{m}$, are used to study the characteristics of the EIT. Figs. 12 show the experimental (dots) and simulation (black lines) power transmission by comparing the spectra of the propagated pulses with and without the cavities. The metal is set as a perfect electrical conductor in the simulation due to the disregard for the attenuation loss of the metal in the THz range. At least 3 more observations may be inferred by looking at Figs. 12; (i), Fig. 12 exhibits a complete loss of spectral power up to the cutoff frequencies of 0.244, 0.236, 0.202, and 0.192 THz, corresponding to $S = 610, 670, 740,$ and $780 \mu\text{m}$, respectively. The water-vapor absorption lines can also be found (0.557 THz) in Figs. 12; (ii), As $S = 610 \mu\text{m}$, the transmission shows strong EIT effect. When S is increased from $610 \mu\text{m}$ to $780 \mu\text{m}$, the low asymmetric resonance shows red-shift. The asymmetric resonant frequencies for $S = 610, 670, 740,$ and $780 \mu\text{m}$ are 0.395, 0.379, 0.354, and 0.338 THz,

respectively. This red-shift of high symmetric resonances can also be found for $S = 610$ and $670 \mu\text{m}$, where the resonant frequencies are 0.456 and 0.446 THz , respectively; (iii) As S is increased to $740 \mu\text{m}$, the main symmetric resonance is degenerated in Fig. 12 (c). This effect can also be found when S is equal to $780 \mu\text{m}$. The measured and simulated results show good agreements. The deviation of experimental and numerical results is probably caused by the imperfections in the fabrication in real structures, which introduces further rearrangement of resonant frequencies.

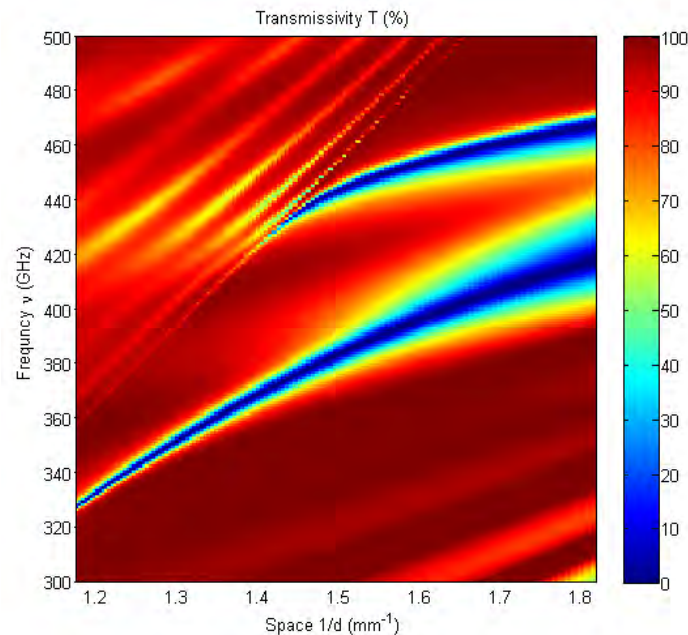


Fig. 13 The 2-dimension transmission map for two cavities with $L = 200 \mu\text{m}$.

To understand the characteristic of the EIT change, in Fig. 13 we report the two dimensional transmission map for the PPWG cavities used in the measurement, obtained by varying incident frequency and waveguide spacing ($1/S$). In Fig. 13, S of 610 , 670 , 740 , and $780 \mu\text{m}$ are shown ($1/S = 1.64$, 1.49 , 1.35 , and 1.28 mm^{-1}) in the experiment, respectively. We can describe the mechanism of manipulation of EIT in PPWG cavities system. By fixing appropriate shifting length L ($200 \mu\text{m}$), as S increases and the two FP resonant wavelengths are larger than S (below the light line), EIT can be found obviously and the two resonances (including the transparent peak) show red-shift. Once the symmetric FP resonant wavelength is less than S , EM wave propagates along a “zigzag line” and acts as guided wave. The cavities produce little influence on the transmission (that is, FP resonance cannot exist in the region above light line). Here the increase of S converts the FP resonance into guided wave. Since the EIT transparent peak between two resonances comes from the destructive interference of symmetric and asymmetric resonances, as the transition of symmetric FP resonance takes place, this interference is broken and an on-to-off EIT peak modulation can be achieved in this process. The mechanism of above manipulation is different from control of EIT in metamaterial and plasmonics. In addition, active electrical manipulation of EIT can also be achieved by using a piezo-actuator in order to adjust waveguide spacing using the voltage source.

5. Frequency selective surface [9]

Originally Frequency selective surface (FSS) is widely used in microwave as a filter for freely propagating waves and now, it has become a promising candidate for the high performance THz filters and THz wave plates owing to its ‘openness’. FSS is a two-dimensional periodic array of resonating metallic-dielectric units, which used to be adopted as filtering elements for free-space radiation. The basic resonating structures of the FSSs include split-ring (SRRs), electric LC (ELC), cut wire, slots, bent-lines, cross lines etc. The “openness” of FSS on geometry makes it easy to integrate different functional structures into a chip to realize multi-functional resonating. In our study [23], a switchable polarization sensitive FSS THz filter is designed and fabricated on a flexible substrate. Its filtering properties are investigated with both simulations and experiments and the results matched well. Furthermore, based on the results, several potential applications of the device were also proposed.

The structure of the resonating units of the FSS filter is shown in Fig. 14, where each unit comprises 4 square ELC structures and 2 connecting bent-lines. To enable such device to work in the THz range, the unit size of the FSS is set to be $200\ \mu\text{m}$ (Wood’s Anomaly appears around $1.3\ \text{THz}$), and the widths of all the lines are set to be $7\ \mu\text{m}$. The side length of the ELC resonator square is $41\ \mu\text{m}$ ($L_{\text{ELC}} = W_{\text{ELC}}$), and the length of the stripe line (one arm of the bent-line structure) is $74\ \mu\text{m}$ ($W_{\text{ELC}} (41\ \mu\text{m}) + L_c (33\ \mu\text{m})$). The FSS is polarization dependent with the connecting bent-lines. We define the polarization angle as illustrated in Fig. 14. The fabrication for the FSS device is taken on a Polyimide (PI) substrate, which is at a low cost but among best choices for THz passive devices fabrication and will be removed from Si wafer after fabrication with the normal semiconductor processing technology. In this letter, the thicknesses of the PI substrate and the copper layer are $21\ \mu\text{m}$ and $2\ \mu\text{m}$, respectively. The whole size of the FSS device is $1\ \text{cm} \times 1\ \text{cm}$. The fabricated FSS device is mounted on a metal holder with a square hole at its center and the size a little smaller than the proposed FSS sample (pFSSs), which makes it good for THz transmittance measurement.

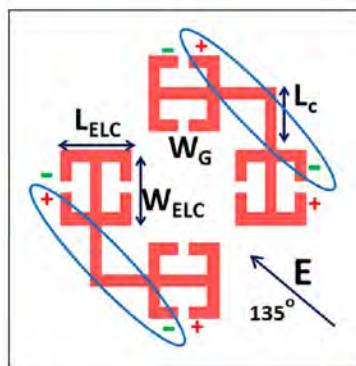


Fig. 14 A unit structure of the FSS sample.

A THz-time domain spectroscopy (TDS) system is applied to characterize the pFSSs. The setup is similar to our previous work, where a homemade GaAs:O bow-tie antenna is pumped by an $800\ \text{nm}$ femto-second (fs) laser to generate THz radiations. The wire-grid polarizer used in the

measurement set-up is tilted at a small angle to incident THz wave to minimize the multi-reflection.

To obtain the polarization dependence of pFSSs, the transmission spectra is measured with the intervals of 5 degrees in experimental measurement. Fig. 2(a) shows the measured pFSSs transmission spectra. The pFSSs transmission properties are also simulated with the full-wave electromagnetic (EM) simulation software: CST Microwave Studio. (Note: Drude model of the copper is used for simulation, where $\omega_p = 1.12 \times 10^{16}$ (rad/s), $\omega_\tau = 2.2 \times 10^{12}$ (1/s)). Both the simulated and experimental results are shown in Fig. 15, which exhibits good consistency although with some differences in the polarization dependence, such consistency is clear in the region from 0.4 to 1 THz. The difference between the simulated and experimental results is mainly due to three folds; 1) the pFSSs is not perfectly perpendicular to the THz beam during the measurement; 2) in simulation, the FSS device size is assumed to be infinite, which means it is periodically expanded without limitation. However, the real pFSSs' size is only $1 \text{ cm} \times 1 \text{ cm}$, i.e., hence the boundary effect can not be neglected since the reflections of evanescent wave at the edge of the sample on the surface can make the resonance peak a little broader than the simulated one; 3) The transmission dip around 0.75 THz and 1.1 THz in Fig. 14 come from the vapor absorption.

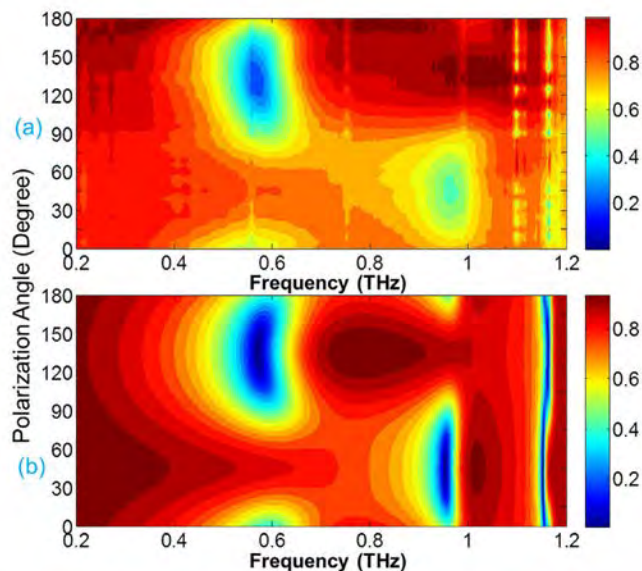


Fig. 15 (a) The measured transmission spectra of the FSS device. (b) The simulated transmission spectra of the FSS device.

As mentioned above, the measurement results prove that the FSS device has good polarization dependent characteristics. When the polarization angle of the FSS device is set to 135° , one can get a reflection resonance peak at 0.57 THz from the simulation, as shown in Fig. 15 (b), and at 0.56 THz from the experiment, as shown in Fig. 15 (a) respectively. This tiny difference is from the measurement deviation as mentioned. In addition, when the polarization angle is changed to 45° , the resonant peak at 0.57 THz disappears, and a new reflection resonance peak appears at

around 0.94 THz. For normal polarization angles (0, 90, 180 degrees.), the device has more than one resonant peaks in the range from 0.5 to 1 THz, and all these angles have the same transmission spectra, owing to the symmetry of proposed device.

The scheme of applying FSS device to THz wave polarization dependent filtering is proposed in this letter. The FSS device is fabricated on a flexible PI substrate with a copper layer, and the polarization selective transmission is achieved successfully. At 45° polarization angle, the simulations show that the FSS device performed like a 4 ELC resonators without connecting bent-line. And at 135° polarization angle, a resonance peak appeared at 0.57 THz because of the offset of resonant charges via the bent-lines. Such characteristics of the device are verified by the experiment as well. Furthermore, the joint areas can be inserted into the FSS structure for an active frequency selection. The relation between the conductivity of the joint areas and the resonant peak position/strength is analyzed by the CST software. This feature is useful for the fabrication of narrow band polarization modulator.

6. Conclusions

In this paper, we have reviewed mode splitting in four useful and easily fabricated THz functional devices. Firstly, we have mentioned the metal holes array, which is fabricated on the aluminum slab. As the varying of incident angle, the lowest mode splits into two branches. Besides, the boundary condition and periodical extension also affect the transmission characteristics. Then, we have mentioned the silicon-based resonance system. Three transmission peaks observed in the experiment is the product of mode splitting and hybrid. This structure can be used as a THz wavelength division multiplexing. Afterwards, we have described the PPWG, which is of EIT-like effect. The two transmission dips observed in experiment are caused by the asymmetrically and symmetrically coupling between top and bottom cavities. Results indicate that the displacing of two cavities and the waveguide spacing affect the frequency location of transmission dips and the existence of higher mode. Eventually, a frequency selective surface based on split-ring and electric LC has been investigated by experimental and simulated methods. The result shows that sample we have studied is a potential high-quality device for narrow band polarization modulating purpose.

Acknowledgements

This work is partly supported by National Program on Key Basic Research Project of China (973 Program, 2014CB339806), the Shanghai Basic Research Key Project (12JC1407100) from Shanghai Committee of Science and Technology, the Major National Development Project of Scientific Instrument and Equipment (2011YQ150021, 2012YQ140005), the Key Scientific and Technological Project of Shanghai Municipality (12142200100), Program for New Century

Excellent Talents in University of Ministry of Education of China (NCET-12-1052), National Natural Science Foundation of China (11174207) (61138001) (61205094), and the Leading Academic Discipline Project of Shanghai Municipal Government (S30502).

References

- [1] B. Ferguson and X. C. Zhang. "Materials for terahertz science and technology". *Nature materials* 1, 26-33 (2002).
- [2] P. H. Siegel. "Terahertz technology". *IEEE Trans. Microwave Theory Tech.* 50(3), 910–928 (2002)
- [3] S. Biber, A. Hofmann, R. Shulz, et. al.. "Design and measurement of a bandpass filter at 300 GHz based on a highly efficient binary grating. Microwave Theory and Techniques". *IEEE Trans. Microwave Theory Tech.* 52(9), 2183–2189 (2004).
- [4] J. He, P. Liu, Y. He, et. al.. "Narrow bandpass tunable terahertz filter based on photonic crystal cavity". *Appl. Opt.* 51(6), 776–779 (2012).
- [5] D. Wu, N. Fang, C. Sun, et. al.. "Terahertz plasmonic high pass filter". *Appl. Phys. Lett.* 83(1), 201–203 (2003).
- [6] I. H. Libon, S. Baumgartner, M. Hempel, et. al.. "An optically controllable terahertz filter". *Appl. Phys. Lett.* 76(20), 2821–2823 (2000).
- [7] H. Li, S. Q. Du, L. Xie, et. al.. "Identifying Radix Curcumae by Using Terahertz Spectroscopy". *Optik* 123, 1129 (2012).
- [8] S. Q. Du, H. Li, L. Xie, et. al.. "Vibrational frequencies of anti-diabetic drug studied by terahertz time-domain spectroscopy". *Appl. Phys. Lett.* 100, 143702 (2012).
- [9] K. J. Chen, Z. Li, J. J. Liu, et. al.. "A Study of FSS in Terahertz Range for Polarization Modulation Purpose". *IEEE Photonics Techn. Lett.* 25, 1613 (2013).
- [10] J. J. Li, X. F. Zang, J. F. Mao, et. al.. "Overlapped optics induced perfect coherent effects". *Scientific Reports* 3, 3569 (2013).
- [11] Y. M. Zhu, T. Unuma, K. Shibata, et. al.. "Femtosecond Acceleration of Electrons under Very High Electric Fields in Bulk GaAs Investigated by Time-Domain Terahertz Spectroscopy". *Appl. Phys. Lett.* 93, 042116 (2008).
- [12] Y. M. Zhu, T. Unuma, K. Shibata, et. al.. "Power Dissipation Spectra and Terahertz Intervalley Transfer Gain in Bulk GaAs under High Electric Fields". *Appl. Phys. Lett.* 93, 232102 (2008).
- [13] Y. M. Zhu, L. Chen, Y. Peng, et. al.. "Temperature Dependence of Nonequilibrium Transport Time of Electrons in Bulk GaAs Investigated by Time-Domain Terahertz Spectroscopy". *Appl. Phys. Lett.* 99, 022111 (2011).
- [14] Y. M. Zhu and S. L. Zhuang. "Terahertz electromagnetic waves emit from semiconductor investigated by time domain terahertz spectroscopy". *Chinese Optics Letters* 9, 110007 (2011).
- [15] J. M. Xu, L. Chen, L. Xie, et. al.. "Effect of Boundary Condition and Periodical Extension on Transmission Characteristics of Terahertz Filters with Periodical Hole Array Structure Fabricated on Aluminum Slab".

Plasmonics 8, 1293 (2013).

- [16] L. Chen, Y. M. Zhu, X. F. Zang, et. al.. “Mode splitting transmission effect of surface wave excitation through a metal hole array”. *Nature: Light Sci. Appl.* 2, e60 (2013).
- [17] J. M. Xu, L. Chen, X. F. Zang, et. al.. “Triple-channel terahertz filter based on mode coupling of cavities resonance system”. *Appl. Phys. Lett.* 103, 161116 (2013).
- [18] J. A. Zhu, L. Chen, J. M. Xu, et. al.. “Theoretical Study of W-shaped Optical Fiber with a Depression in Core Center by Applying Analytical Transfer Matrix Method”. *Opt. Commun.* 284, 5130 (2011).
- [19] L. Chen, C. M. Gao, J. M. Xu, et. al.. “Observation of electromagnetically induced transparency-like transmission in terahertz asymmetric waveguide-cavities systems”. *Opt. Lett.* 38, 1379 (2013).
- [20] L. Chen, J. M. Xu, C. M. Gao, et. al.. “Manipulating terahertz electromagnetic induced transparency through parallel plate waveguide cavities”. *Appl. Phys. Lett.* 103, 251105 (2013).
- [21] X. F. Zang, T. Zhou, B. Cai, et. al.. “Single-photon transport properties in an optical waveguide coupled with a Λ -type three-level atom”. *J. Opt. Soc. Am. B* 30, 1135 (2013).
- [22] X. F. Zang, T. Zhou, B. Cai, et. al.. “Controlling Single-photon Transport Properties In a Waveguide Coupled With Two Separated Atoms”. *J. Phys. B* 46, 145504 (2013).